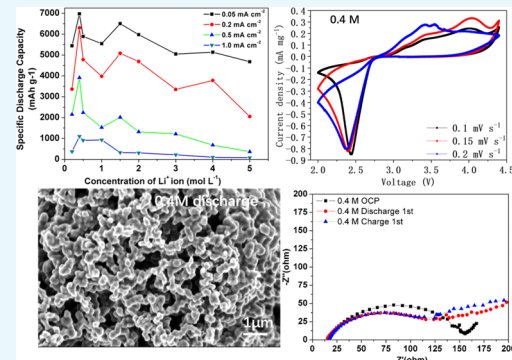


# LiTFSI Concentration Optimization in TEGDME Solvent for Lithium–Oxygen Batteries

Jingwen Chen,<sup>†</sup> Chunguang Chen,<sup>‡</sup> Tao Huang,<sup>\*,†</sup> and Aishui Yu<sup>\*,†,‡</sup>

<sup>†</sup>Laboratory of Advanced Materials and <sup>‡</sup>Department of Chemistry, Shanghai Key Laboratory of Molecular Catalysis and Innovative Materials, Collaborative Innovation Center of Chemistry for Energy Materials, Fudan University, Shanghai 200438, China

**ABSTRACT:** Focus on lithium–oxygen batteries is growing due to their various advantages, such as their high theoretical energy densities and renewable and environmentally friendly characteristics. Nonaqueous organic electrolytes play a key role in lithium–oxygen batteries, allowing the conduction of lithium ions and oxygen transfer in the three phase boundaries (cathode–gas–electrolyte). Herein, we report the effect of lithium salt concentrations in single-solvent lithium–oxygen battery systems systematically (using bis(trifluoromethanesulfonyl)imide (LiTFSI) in tetraethylene glycol dimethyl ether (TEGDME)) on their electrochemical performances. The first discharge capacities and cyclabilities exhibit favorable correlations with the lithium salt concentration, of which using 0.4 and 1.5 M LiTFSI show the best discharge capacities and cyclabilities. The specific capacity of the 0.4 M LiTFSI system reaches 7000 mAh g<sup>-1</sup>, about 1.3 times that of the commonly used 1 M LiTFSI in TEGDME. Cyclic voltammetry with slow scan speeds further investigates the system stability and reaction mechanism. The surface morphology after the discharge and interface impedance after charging, which are examined using scanning electron microscopy (SEM) and electrochemical impedance spectroscopy (EIS), have significant effects on the comprehensive performances. Conductivity and viscosity play mutual roles in the lithium–oxygen battery performance, while the oxygen solvation has little effect.



## 1. INTRODUCTION

Since Abraham invented the lithium–oxygen battery in 1996, it has been studied worldwide.<sup>1</sup> Lithium–oxygen batteries are viewed as the next generation of new energy batteries for this century because of their ultrahigh theoretical energy densities, which are nearly equal to those of gasoline; capacity density; and environmentally friendly characteristics.<sup>2–4</sup> However, the practical application of lithium–oxygen batteries is limited due to many issues, such as formation of dendritic lithium anodes with cycling procedure,<sup>5–7</sup> the adsorption and storage of the active material on the positive oxygen electrode,<sup>8–10</sup> and electrolyte optimization and volume utilization. Especially, for the last part, researchers have put forward a series of electrochemical systems for stable lithium salt and solvent adaptation, which can be examined by theoretical models and calculations<sup>11–14</sup> and experimental research studies, such as Fourier-transform infrared (FTIR) spectroscopy,<sup>15,16</sup> Raman spectroscopy,<sup>17,18</sup> electrochemical impedance spectroscopy (EIS),<sup>19–22</sup> and scanning electron microscopy (SEM).<sup>23,24</sup> About optimizing the electrolytes, this can be achieved by introducing appropriate organic additives, soluble reduction catalysts, but all of these strategies are based on complete improvement of the basic electrolyte mechanism.<sup>25–27</sup> Recently, Francesca et al. explored different bis(trifluoromethanesulfonyl)imide (LiTFSI) to tetraethylene glycol dimethyl ether (TEGDME) molar ratios with the oxygen reduction reaction (ORR) mechanism explaining the Li<sub>2</sub>O<sub>2</sub> product formation. They emphasized the dynamic

influence of oxygen solubility toward a superconcentrated solution; however, they ignored the influence of anode Li<sup>+</sup> ion conductivity and cathode product surface morphologies.<sup>28</sup> Garcia et al. investigated the various LiTFSI in DME and studied Li<sup>+</sup> ion conductance, cathode interface impedance, and electrolyte decomposition, which have a direct impact on efficiency. The research supplemented the theoretical calculation method but ignored the effects of discharge capacity and cathode Li<sub>2</sub>O<sub>2</sub> specific morphologies.<sup>29</sup> Zhou et al. explored the LiTFSI concentrations in glymes and used the optimized molar ratio of 1:5 in the system, which exhibited excellent cycling performance, but the basic physical properties of the electrolyte were not considered clearly, and the given reaction mechanism interpretation for applied chemistry data was not enough.<sup>30</sup> Gittleson et al. discussed the influence of oxygen in lithium–oxygen batteries in different systems, implying that oxygen influences the performances systemically.<sup>31</sup> Klassen et al. studied the optimal LiClO<sub>4</sub> concentration in carbonate solvents but only optimized the design for conductivity. LiClO<sub>4</sub> in organic solvents exhibits poor cyclability, and its physical properties are inadequate.<sup>32</sup> Zhang et al. suggested an optimal LiTFSI concentration in propylene carbonate/ethylene carbonate (PC/EC) of 0.8 M to obtain the maximum discharge capacity, and they also studied high concentrations

Received: September 10, 2019

Accepted: November 13, 2019

Published: November 26, 2019

of LiTFSI in DME and found that lithium–oxygen batteries exhibited greater capacities with 3 M LiTFSI, and the advantage is even more pronounced for cyclability.<sup>33,34</sup> However, they did not focus on the influence of high LiTFSI concentrations on the oxygen cathode. Liu et al. examined the morphology of the cathode over a wide range of lithium concentrations of LiTFSI in TEGDME.<sup>35</sup> They achieved an explanation of cathode  $\text{Li}_2\text{O}_2$  images but with incomplete concentrations, and they only find one peak for  $\text{Li}-\text{O}_2$  batteries. The charge–discharge reaction mechanisms have been studied with the products and byproducts being explored extensively.<sup>36–38</sup> It has been found that TEGDME has a low DN (the Gutmann donor number (DN), which is an index of Lewis basicity and important for the equilibrium), following the  $\text{Li}_2\text{O}_2$  surface phase mechanism, and exhibits a low discharge capacity and good cyclability.<sup>39</sup> However, bis-(trifluoromethanesulfonyl)imide (LiTFSI) has been found to be a high-DN salt, and solvation of the  $\text{Li}^+$  ions has a significant effect. McCloskey verified that the  $\text{TFSI}^-$  ion concentrations have little influence on the performance, particularly for the discharge capacity, as it did not influence the  $\text{Li}^+$  solvation process.<sup>40</sup> Electrochemical differential mass spectrometry (DEMS) analysis of the  $\text{Li}_2\text{O}_2$  products and decomposition of the electrolyte suggested that TEGDME is more stable than any other solvents such as amines and esters.

In our work, we choose a Ketjenblack 600 (KB carbon) electrode as it has a high capacity with poly-(tetrafluoroethylene) (PTFE), which is an excellent binder commonly used for best match empirically, and because of its adaptability to the better electrolytic liquid system LiTFSI in TEGDME. Therefore, although the whole research system becomes complicated, the research results are still of high reference value for the lithium–oxygen battery due to its excellent performance. We discussed the first discharge capacity with different current densities and selected the appropriate charge–discharge current density of  $0.2 \text{ mA cm}^{-2}$  to compare the Coulombic efficiency and cyclabilities. EIS and SEM are used to evaluate the performances of lithium–oxygen batteries about electron transfer impedance and product morphology effects. We studied the physical properties, viscosity, ion conductivity, and oxygen solubility, for different LiTFSI concentrations in TEGDME. Through measurements of the electrolytes, we found that the viscosity and lithium ion conductivity are the main influencing factors, regardless of the oxygen solubility. To study that the viscosity increase has nearly no effect on the electrochemical performances, we use cyclic voltammetry with slow scan rates to evaluate the electrochemical reaction process. Obviously, both system stability and changes in products  $\text{Li}_2\text{O}_2$  morphologies compensate for the negative effect of viscosity increase with an increase in LiTFSI concentrations. By comprehensively studying the effect of physicochemical properties on the battery performances, we provide suggestions on how to optimize the electrolyte for lithium–oxygen batteries at low or high concentrations.

## 2. EXPERIMENTAL SECTION

**2.1. Electrolyte Preparation.** The lithium salt LiTFSI and the TEGDME (98% volume concentration) solvent were purchased from Sigma-Aldrich. Activated molecular sieves ( $4 \text{ \AA}$ ) were immersed in the aforementioned solvent for 3 days to remove residual water before use. The concentrations of the prepared electrolytes were 0.2, 0.4, 0.5, 1, 1.5, 2, 3, 4, and 5 M.

**2.2. Air Cathode Preparation and Cell Assembly.** KB carbon and 20 wt % poly(tetrafluoroethylene) (PTFE) were mixed (8:2 by weight) in an ethanol-based solution. After stirring thoroughly, the slurry was coated on nickel foam with a diameter of 12 mm. The cathode was subsequently dried in a vacuum oven for 12 h at  $80^\circ\text{C}$  to remove residual ethanol. After vacuum-drying, the typical carbon loading was  $0.6 \pm 0.2 \text{ mg cm}^{-2}$ . Li foil ( $\varnothing 15 \times 0.6 \text{ mm}^2$ ), a Celgard 3500 membrane, waterleaf paper, and a porous air electrode with different LiTFSI concentrations of the electrolyte (about  $50 \mu\text{L}$ ) were used to assemble the cells. All of the batteries were assembled in an Ar atmosphere glovebox ( $\text{H}_2\text{O} \leq 1 \text{ ppm}$ ,  $\text{O}_2 \leq 1 \text{ ppm}$ ) utilizing Swagelok batteries with an air window of  $78.5 \text{ mm}^2$ .

**2.3. Measurements.** The viscosity, ionic conductivity, and the oxygen solubility of the electrolytes were measured using a viscometer (DV2TLVT), conductivity meter (S230-USP/EP), and dissolved oxygen probe (10 FT Cable/EA) at  $25^\circ\text{C}$ , respectively. Before measuring the oxygen solubility, the system was oxygenated for 10 min to ensure oxygen saturation.

The cyclic voltammetry (CV) curves were obtained galvanostatically using Metrohm Autolab B.V. (Utrecht, the Netherlands). The scan rates were 0.1, 0.15, and  $0.2 \text{ mV s}^{-1}$  from an open-circuit potential (about 3.0 V) to 2.0 V, after which the batteries were charged to 4.4 V and returned to the open-circuit potential. The charge–discharge profile measurements of the  $\text{Li}-\text{O}_2$  batteries were obtained galvanostatically using a LAND BT2000 battery test system (Wuhan Land Electronic Co. Ltd., China). The first discharge capacities were obtained such that the discharge voltages were limited to 2.0 V, and the charge step ended when the charge voltage increased to 4.4 V with constant current densities of 0.05, 0.2, 0.5, and  $1.0 \text{ mA cm}^{-2}$  with different concentrations of LiTFSI in TEGDME. To investigate the rate capabilities of the cells, charge–discharge steps were carried out similarly to those in the first discharge capacity tests. The cyclabilities were measured when discharge capacities were limited to  $500 \text{ mAh g}^{-1}$ , and the charge step ended when the charge voltage increased to 4.4 V at the specific current density of  $0.2 \text{ mA cm}^{-2}$  with different concentrations of electrolytes. Moreover, we examined the full battery performance at  $0.2 \text{ mA cm}^{-2}$  to explain the results thoroughly. EIS measurements using lithium–oxygen batteries were performed to measure the interfacial resistances in the frequency range of 100 kHz to 1 Hz with an amplitude of 5 mV. All electrochemical tests were performed in gloveboxes filled with oxygen.

Field-emission scanning electron microscopy (FESEM, Hitachi S4800) was applied to observe the morphologies of the electrode surfaces.

## 3. RESULTS AND DISCUSSION

**3.1. Physical Properties of Different LiTFSI Concentrations in TEGDME.** Physical characterization with different concentrations of electrolytes was performed first (Figures 1 and 2). As shown in Figure 1, the conductivities of the electrolytes containing different concentrations of LiTFSI in TEGDME went through a maximum and subsequently decreased as the Li concentration increased, and the peak value appeared at 1.0 M (about 2.72 mS).

As shown in Figure 2, the viscosity exhibited no obvious change below 1 M LiTFSI. The electrolyte viscosity slightly increased between 1 and 2 M. Above 2 M, a remarkable increase in the electrolyte viscosity was observed, which was

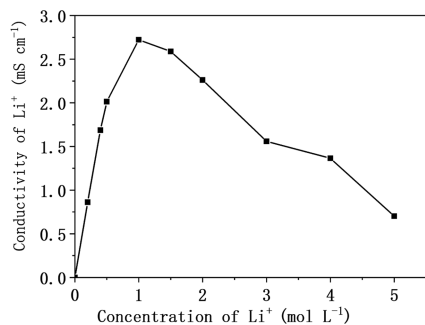


**Figure 1.** Ionic conductivity with LiTFSI concentrations of 0.2, 0.4, 0.5, 1, 1.5, 2, 3, 4, and 5 M in the TEGDME electrolyte.

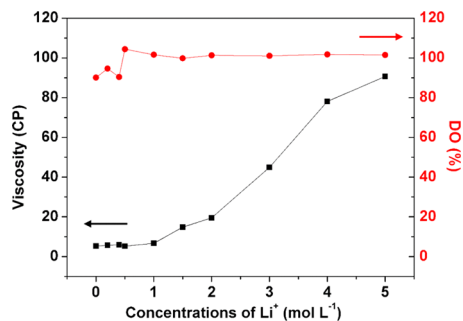


**Figure 2.** Viscosity and DO % for LiTFSI concentrations of 0.2, 0.4, 0.5, 1, 1.5, 2, 3, 4, and 5 M in the TEGDME electrolyte.

ascribed to the cluster formation of Li ions with TEGDME molecules of the solvent. The dissolved oxygen values for different concentrations of electrolyte showed two regions. Below 0.5 M, the dissolved oxygen content was approximately about 90%, while it was approximately 100% for 0.5 M and higher concentrations. The properties influence the battery performances distinctly. First, a high Li ionic conductivity guarantees lithium ion transport through the entire battery (usually above 1 mS cm<sup>-1</sup>). That is, both small bounds besides 1 M have good Li<sup>+</sup> ion conductivity. As the LiTFSI concentrations increase, the viscosity affects a lot, whereas the oxygen solubility has little effect. Obviously, the rapid increase of viscosity caused by high LiTFSI concentration slows down the absorption and desorption of lithium, which may contribute to the loss of capacity. Moreover, the oxygen solubility value increased slightly with LiTFSI concentrations caused by F atom in TFSI<sup>-</sup>.

**3.2. Reaction Mechanism.** As shown in Figure 3a, we utilized the minimum scan rate to ensure that the oxygen was dissolved in the TEGDME. The lithium–oxygen batteries were discharged to 2.0 V and charged to 4.4 V for the charge–discharge process. At extremely slow scan rates, we determined the reaction mechanism. Evidently, at a 0.1 mV s<sup>-1</sup> scan rate, the 4 and 5 M LiTFSI systems exhibited a significantly larger cathode area, which indicates that there was apparent irreversibility. This could be attributed to the instability of the system and decomposition of the electrolytes. For 0.2 or 3 M LiTFSI, the anode peaks moved and were wider than those at other concentrations, corresponding to the slow rate reduction reaction. In this reaction, oxygen was first reduced with Li<sup>+</sup> ions to Li<sub>2</sub>O and then to Li<sub>2</sub>O<sub>2</sub>. The defects formed during the slow reaction may be attributed to Li<sub>2</sub>O<sub>2</sub> nucleation hysteresis from the dissolved Li<sub>2</sub>O, which itself requires a high voltage to decompose, resulting in positive hole plugging and

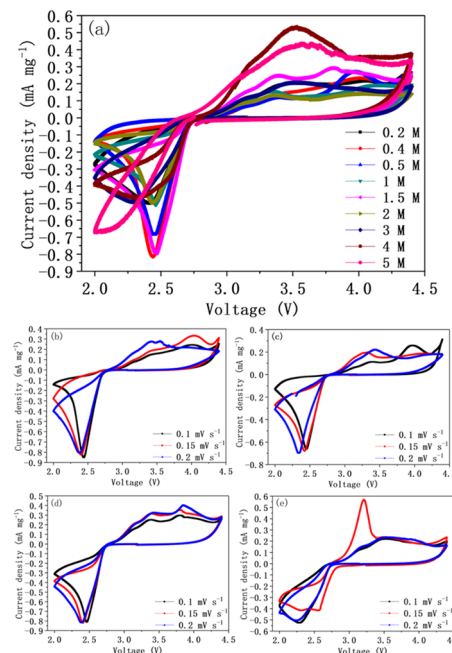


**Figure 3.** (a) First cyclic voltammetry (CV) at a 0.1 mV s<sup>-1</sup> scan rate for LiTFSI concentrations of 0.2, 0.4, 0.5, 1, 1.5, 2, 3, 4, and 5 M. First CV curves for 0.1, 0.15, and 0.2 mV s<sup>-1</sup> scan rates with (b) 0.4 M LiTFSI, (c) 0.5 M LiTFSI, (d) 1.5 M LiTFSI, and (e) 3 M LiTFSI in TEGDME.

bad cyclability. As for other LiTFSI concentrations, the reduction peaks were relatively consistent at nearly 2.45 V (corresponding to reduction of O<sub>2</sub> to Li<sub>2</sub>O<sub>2</sub>), but the number of oxidation peaks increased from one (at nearly 3.5 V corresponding to oxidation of Li<sub>2</sub>O<sub>2</sub>) to two (at nearly 3.5 and 4.0 V corresponding to oxidation of Li<sub>2</sub>O<sub>2</sub> and Li<sub>2</sub>O, respectively) with the increase in the LiTFSI concentration. This also indicates that the two oxygen evolution reactions separate while increasing the LiTFSI concentration. This occurs because of the increased Li<sup>+</sup> concentration, causing Li<sub>2</sub>O to form more easily. At this slow scan rate, we observed oxidation peak separation.

To investigate the influence of the LiTFSI concentrations on the Li–oxygen battery reaction mechanism in TEGDME, we performed CV at low scan rates (0.1, 0.15, and 0.2 mV s<sup>-1</sup>) using 0.4, 0.5, 1.5, and 3 M LiTFSI. The reaction mechanism was very complex, as shown in Figure 3b–e. However, we confirmed that the anode peak potential value shifted toward a relatively stable lithium–oxygen battery system, and this shift was in the negative direction. This means that there were adequate oxygen and Li<sup>+</sup> in the whole system. The cyclic voltammetry behaviors were valuable for practical lithium–oxygen battery systems because the charge–discharge current densities for the present lithium–oxygen batteries were smaller than those of traditional lithium ion battery systems. At 0.4 and 1.5 M LiTFSI, the peak position offset is relatively small with the increasing scan speed. However, by the same amplitude scan rate increased, whether at 0.5 and 3 M, the shift in the peak position is uncertain or even reversed. Obviously, the system state is relatively stable at 0.4 and 1.5 M LiTFSI. This is just a reference for the stability of our battery system; however, the specific peaks are more complex and not discussed in detail.

**3.3. First Discharge Capacity.** The first discharge capacities were measured from the open-circuit voltage discharge to 2.0 V and then to 4.4 V. As shown in Figure 4b–j, at the same current density (illustrated for 0.05 mA cm<sup>-2</sup>)

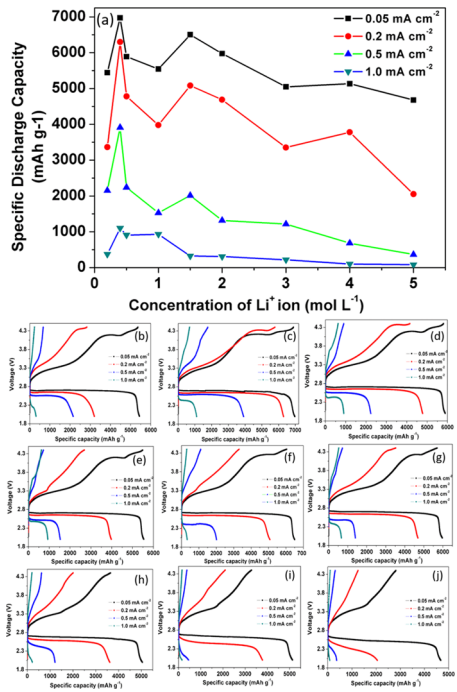


**Figure 4.** (a) First specific discharge capacity for different concentrations of LiTFSI in TEGDME at different discharge current densities from the open-circuit voltage to the terminal voltage at 2.0 V. (b–j) First charge–discharge curves for different LiTFSI concentrations ((b) 0.2 M, (c) 0.4 M, (d) 0.5 M, (e) 1 M, (f) 1.5 M, (g) 2 M, (h) 3 M, (i) 4 M, and (j) 5 M) in TEGDME at charge–discharge current densities of 0.05, 0.2, 0.5, and 1 mA cm<sup>-2</sup>.

cm<sup>-2</sup>), the order of first specific discharge capacities from highest to lowest was 0.4 M LiTFSI (nearly 7000 mAh g<sup>-1</sup>), 1.5 M (nearly 6500 mAh g<sup>-1</sup>), the lower concentrations (about 5700 mAh g<sup>-1</sup>), and the higher concentrations (exhibited attenuation trends from 2 to 5 M, beginning at nearly 6000 mAh g<sup>-1</sup> and decreasing to 5000 mAh g<sup>-1</sup> in 5 M LiTFSI). Moreover, the specific discharge capacity variation tendency was nearly consistent at other current densities. Thus, at the same LiTFSI concentration, the discharge capacity decreases gradually with increasing discharge–charge current density. Furthermore, the first specific discharge capacity decreased with the increase in the discharge–charge current density, which was more evident between 0.2 and 0.5 mA cm<sup>-2</sup> at different charge–discharge current densities. The comparison is shown in Figure 4a.

**3.4. Rate Ability.** As shown in Figure 5, the different constant charge–discharge current densities resulted in evident differences at different LiTFSI concentrations. At the lowest current density of 0.05 mA cm<sup>-2</sup>, the efficiency could be distinguished between the 2 M LiTFSI (nearly 100%) and the higher concentrations. As the current density slightly increased, to 0.2 mA cm<sup>-2</sup>, the efficiency toward the lower concentrations was subdivided successfully below 1 M LiTFSI and between 1 and 2 M. This may be ascribed to the higher current density accelerating the differentiation for interface transport impedance, which can be seen in Figure 5. However, at a higher

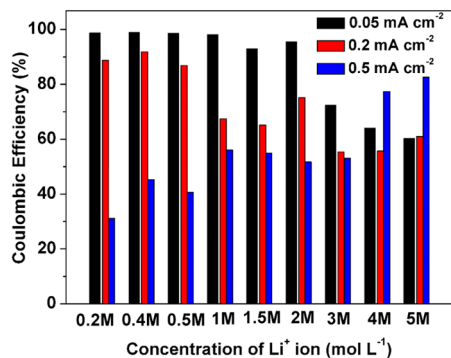


**Figure 5.** Coulombic efficiency with different concentrations of LiTFSI in TEGDME at different constant discharge–charge current densities from the open-circuit voltage to 2.0 V, followed by charging to the terminal voltage of 4.4 V.

current density of 0.5 mA cm<sup>-2</sup>, the behavior changed significantly. The lower concentrations exhibited distinct decreases than other concentrations, and even at the ultrahigh current densities achieved at 4 and 5 M, the efficiency was greater than that at lower current densities. At the lower concentrations, the formation of spherical discharge products may easily block the holes of the cathode during the fast discharge step, preventing the complete decomposition process. However, at higher concentrations, amorphous membrane products formed that could be easily decomposed.

**3.5. Cyclability.** Figure 6 shows the cyclability for different concentrations of LiTFSI in TEGDME with a fixed discharge

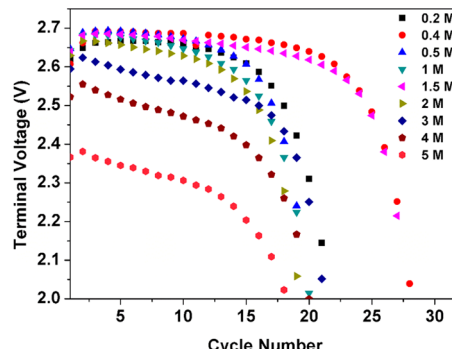


**Figure 6.** Cycling performance based on discharge terminal voltage versus cycle numbers for different concentrations of LiTFSI in TEGDME.

capacity of 500 mAh g<sup>-1</sup> at a current density of 0.2 mA cm<sup>-2</sup>. The terminal voltage for 0.4 and 1.5 M concentrations of LiTFSI (of nearly 2.7 V) exhibited better performances than that for other concentrations (about 28 cycles to reach a terminal discharge voltage of 2.0 V). Besides these two concentrations, the performance at 0.4 M was slightly better than that at 1.5 M, which was evident after 10 cycles. The performances at below 0.4 M concentrations of LiTFSI were better than those at higher concentrations. The results are consistent with the interface transfer impedance and the discharge product morphologies of the cathodes. Also, we consider that in ultrahigh concentration solutions the molar ratio of the organic solvent and Li<sup>+</sup> is nearly the same, and this reduces the Li<sup>+</sup> Lewis acidity, forming a big cation complex Li(TEGDME)<sup>n+</sup>. The complex can reduce the fast LiO<sub>2</sub> disproportion that reduces the cycling performance. However,

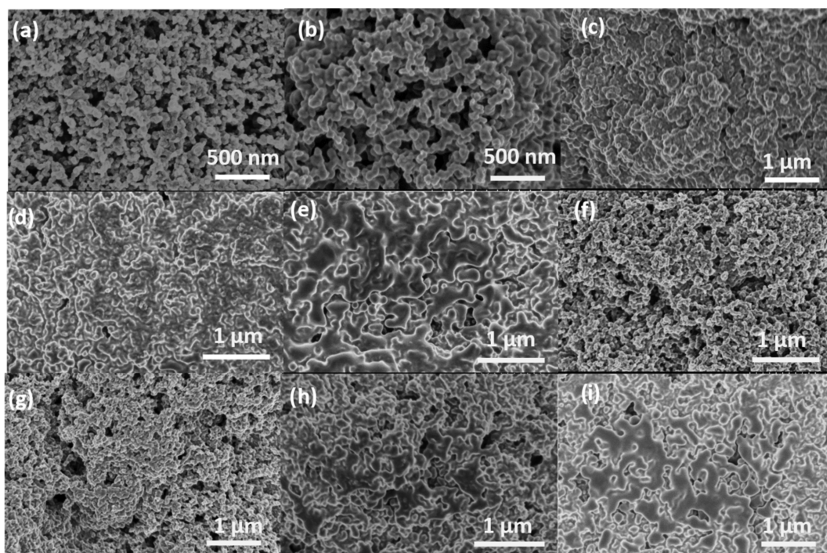


**Figure 7.** (a) SEM images of the KB carbon cathode before discharge. (b–e) Discharged first cathodes at the concentrations of 0.4, 0.5, 1.5, and 3 M and at a constant current density of  $0.2 \text{ mA cm}^{-2}$ . (f–i) Charged first cathodes at the concentrations of 0.4, 0.5, 1.5, and 3 M and at a constant current density of  $0.2 \text{ mA cm}^{-2}$ .

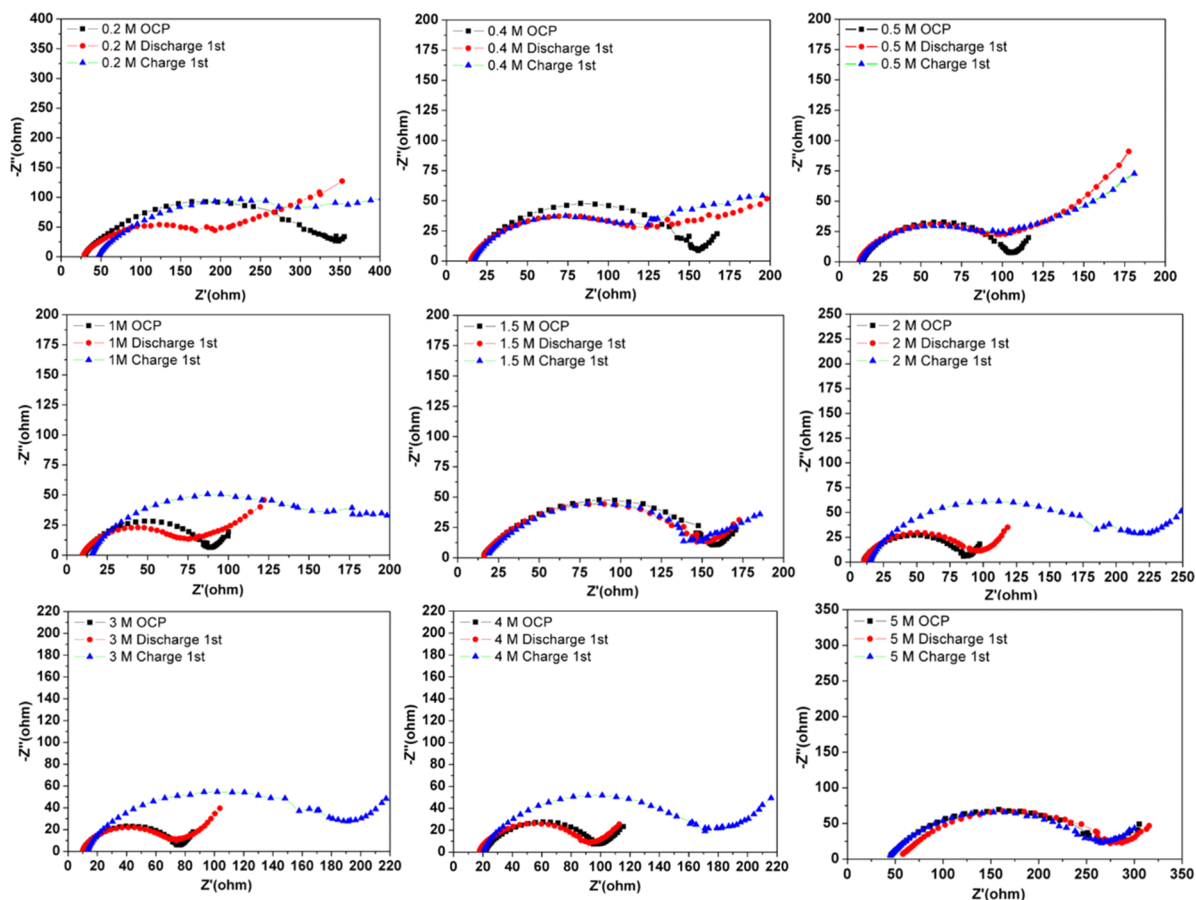


**Figure 8.** EIS spectra of cells at open-circuit voltage, discharged to 2.0 V, and charged to 4.4 V with  $0.2 \text{ mA cm}^{-2}$  current densities and 0.4, 0.5, 1.5, and 3 M concentrations.

LiTFSI at a slightly higher concentration can effectively combine with TEGDME to prevent solvent decomposition and improve the cycling performance. As a result, double peaks exhibit good cycle performance in a Li/LiTFSI–TEGDME/KB-PTFE battery system.

**3.6. SEM and EIS for Full Batteries.** As shown in Figure 7, there were different forms of the discharge products. As shown in Figure 7a, the pristine air cathode (KB electrode) exhibited connected small spherical particles. The holes were evenly distributed. When discharged first to 2 V at a current

density of  $0.2 \text{ mA cm}^{-2}$ , the product particle morphologies are evident. At lower concentrations,  $\text{Li}_2\text{O}_2$  attached to the surface of the KB carbon. The particles grew significantly and covered the spherical KB, which is evident in Figure 7b,c. However, at a concentration of  $1.5 \text{ M}$  or higher, membrane-like products not only covered the surfaces of the KB particles but also distributed in the holes, spreading over the entire cathode, which is evident in Figure 7d–f. The products with higher concentrations were amorphous  $\text{Li}_2\text{O}_2$ , which generally decompose easily during charge processes. Moreover, we tested the morphology for the sample charged first to  $4.4 \text{ V}$ . The  $\text{Li}_2\text{O}_2$  products decomposed for the  $0.4 \text{ M}$  LiTFSI, and the particle sizes were nearly the same as those of the pristine sample. This indicated that there was good OER performance, which led to optimum cyclability. At a  $0.5 \text{ M}$  LiTFSI concentration, the spherical products were larger than those at  $0.4 \text{ M}$ , the sizes of the morphological features were bigger, and  $\text{Li}_2\text{O}_2$  was not fully decomposed. However, at higher concentrations, the membrane-like amorphous  $\text{Li}_2\text{O}_2$ , which spread across the whole cathode, were more easily decomposed at  $1.5 \text{ M}$  than at  $3 \text{ M}$ . Compared with the spherical morphologies, the membrane-like products were amorphous and decomposed nearly completely, leaving small particles similar to those of the pristine sample. Thus, the spherical products formed easily at lower concentrations, but partial overwrapping resulted in decomposition difficulties. The membrane-like products easily decomposed but clogged the pores. As a result,  $0.4$  and  $1.5 \text{ M}$  LiTFSI contributed to good performance in terms of the discharge capacity and cyclability.

As shown in Figure 8, EIS spectra changed at different states. The interface transfer impedance of the pristine sample decreased between the lowest concentration  $0.2 \text{ M}$  and  $1 \text{ M}$  ( $\sim 80 \Omega$ ), after which it rapidly increased to  $1.5 \text{ M}$  ( $\sim 140 \Omega$ ) and subsequently decreased ( $\sim 80 \Omega$ ) between  $2$  and  $4 \text{ M}$ . Finally, it increased rapidly again to  $5 \text{ M}$  ( $\sim 225 \Omega$ ). The results can be explained by the comprehensive physical properties, ionic conductivity, viscosity, and oxygen solubility. The open-circuit voltage interface impedance was not the dominant factor of the lithium–oxygen battery performances. The interface transfer impedance results showed that the best LiTFSI concentration was  $0.4 \text{ M}$ , which decreased effectively after the discharge than at the open-circuit voltage, while after 1 charge cycle, the impedance nearly did not change. This also indicates that the  $\text{Li}_2\text{O}_2$  discharge products were better decomposed at  $0.4 \text{ M}$  LiTFSI in TEGDME. A similar phenomenon can be seen for  $1.5$  and  $0.5 \text{ M}$  LiTFSI, which also decreased the interface impedance, but not for a concentration of  $0.4 \text{ M}$ . However, the lowest and highest concentrations were different. After the discharge step, the interface transfer impedance did not significantly change, and after the charge step, the impedance increased considerably, which contributed to the poor cycle performance.

#### 4. CONCLUSIONS

In our study, we explored that different LiTFSI concentrations with the TEGDME solvent result in different discharge capacities, rate abilities, and cyclabilities. Furthermore, we explained the electrochemical system stability with CV at low scan rates for lithium–oxygen batteries with different LiTFSI concentrations (from  $0.2$  to  $5 \text{ M}$ ) briefly. Moreover, the  $4$  and  $5 \text{ M}$  LiTFSI systems were the most unstable. The  $0.2$  and  $3 \text{ M}$  systems exhibited slow oxygen reduction steps, which contributed to difficulty in decomposition of the  $\text{Li}_2\text{O}_2$  and

$\text{Li}_2\text{O}$  discharge products. As for other LiTFSI concentrations, which exhibited fast oxygen reduction steps, the oxidation peak gradually separated with the increase in LiTFSI concentration, which exhibited better oxygen reduction and product oxidation processes with different product oxidation procedures. Thus, we increased the scan rate slightly to investigate this further. With increasing scan rate, only  $0.4$  and  $1.5 \text{ M}$  LiTFSI concentrations systems show a slight right shift at the peak position of the cyclic voltammetry, which corresponds to a relatively stable system. The specific electrochemical performances are measured. The  $0.4$  and  $1.5 \text{ M}$  LiTFSI systems exhibited better first specific discharge capacities and cyclabilities, which were ascribed to the cathode morphology and interface transfer impedance. The rate abilities at various concentrations were different, but there was no obvious trend as the current density increased. The physical properties of the electrolytes are important, especially the  $\text{Li}^+$  ion conductivity, viscosity, and oxygen solubility. The  $\text{Li}^+$  ion conductivity and viscosity influence the lithium–oxygen battery performances significantly, while the oxygen solubility had little effect. Above all, we focus on acquiring higher primary capacity and better cycle performance, whether little is known about the efficiency problems caused by some byproducts, such as  $\text{LiOH}$ ,  $\text{Li}_2\text{CO}_3$  and the  $\text{TFSI}^-$  decomposition, which could be an additional detailed part to be considered. The surface of lithium anode with different LiTFSI concentration electrolytes has been studied deeply and has an important influence, so we did not discuss this in detail in this article.

#### ■ AUTHOR INFORMATION

##### Corresponding Authors

\*E-mail: huangt@fudan.edu.cn (T.H.).

\*E-mail: asyu@fudan.edu.cn (A.Y.).

##### ORCID ®

Aishui Yu: 0000-0002-8135-5123

##### Notes

The authors declare no competing financial interest.

#### ■ ACKNOWLEDGMENTS

The authors acknowledge financial support from the Natural Science Foundation of Shanghai (19ZR1403600).

#### ■ REFERENCES

- (1) Abraham, K. M.; Jiang, Z. A polymer electrolyte-based rechargeable lithium/oxygen battery. *J. Electrochem. Soc.* **1996**, *143*, 1–5.
- (2) Girishkumar, G.; McCloskey, B.; Luntz, A. C.; Swanson, S.; Wilcke, W. Lithium-air battery: promise and challenges. *J. Phys. Chem. Lett.* **2010**, *1*, 2193–2203.
- (3) Aurbach, D.; McCloskey, B. D.; Nazar, L. F.; Bruce, P. G. Advances in understanding mechanisms underpinning lithium–air batteries. *Nat. Energy* **2016**, *1*, No. 16128.
- (4) Bruce, P. G.; Freunberger, S. A.; Hardwick, L. J.; Tarascon, J.-M.  $\text{Li}-\text{O}_2$  and  $\text{Li}-\text{S}$  batteries with high energy storage. *Nature Mater.* **2012**, *11*, 19–29.
- (5) Lu, Y.-C.; Gallant, B. M.; Kwabi, D. G.; Harding, J. R.; Mitchell, R. R.; Whittingham, M. S.; Shao-Horn, Y. Lithium–oxygen batteries: bridging mechanistic understanding and battery performance. *Energy Environ. Sci.* **2013**, *6*, 750–768.
- (6) Wang, J.; Li, Y.; Sun, X. Challenges and opportunities of nanostructured materials for aprotic rechargeable lithium–air batteries. *Nano Energy* **2013**, *2*, 443–467.

- (7) Kraysberg, A.; Ein-Eli, Y. Review on Li–air batteries—opportunities, limitations and perspective. *J. Power Sources* **2011**, *196*, 886–893.
- (8) Gao, X.; Chen, Y.; Johnson, L.; Bruce, P. G. Promoting solution phase discharge in Li–O<sub>2</sub> batteries containing weakly solvating electrolyte solutions. *Nat. Mater.* **2016**, *15*, 882–888.
- (9) Yang, L.; Frith, J. T.; Garcia-Araez, N.; Owen, J. R. A new method to prevent degradation of lithium–oxygen batteries: reduction of superoxide by viologen. *Chem. Commun.* **2015**, *51*, 1705–1708.
- (10) Matsuda, S.; Hashimoto, K.; Nakanishi, S. Efficient Li<sub>2</sub>O<sub>2</sub> formation via aprotic oxygen reduction reaction mediated by quinone derivatives. *J. Phys. Chem. C* **2014**, *118*, 18397–18400.
- (11) Sharon, D.; Hirsberg, D.; Salama, M.; Afri, M.; Frimer, A. A.; Noked, M.; Kwak, W.; Sun, Y.-K.; Aurbach, D. Mechanistic role of Li<sup>+</sup> dissociation level in aprotic Li–O<sub>2</sub> battery. *ACS Appl. Mater. Interfaces* **2016**, *8*, 5300–5307.
- (12) Kim, D. W.; Ahn, S.; Kang, J.; Suk, J.; Kim, H. K.; Kang, Y. In situ real-time and quantitative investigation on the stability of nonaqueous lithium–oxygen battery electrolytes. *J. Mater. Chem. A* **2016**, *4*, 6332–6341.
- (13) Abraham, K. M. Electrolyte-directed reactions of the oxygen electrode in lithium–air batteries. *J. Electrochem. Soc.* **2015**, *162*, A3021–A3031.
- (14) McCloskey, B. D.; Valery, A.; Luntz, A. C.; Gowda, S. R.; Wallraff, G. M.; Garcia, J. M.; Mori, T.; Krupp, L. E. Combining accurate O<sub>2</sub> and Li<sub>2</sub>O<sub>2</sub> assays to separate discharge and charge stability limitations in nonaqueous Li–O<sub>2</sub> Batteries. *J. Phys. Chem. Lett.* **2013**, *4*, 2989–2993.
- (15) Mozhzhukhina, N.; Méndez De Leo, L. P.; Calvo, E. J. Infrared spectroscopy studies on stability of dimethyl sulfoxide for application in a Li–Air battery. *J. Phys. Chem. C* **2013**, *117*, 18375–18380.
- (16) Yu, Q.; Ye, S. In situ study of oxygen reduction in dimethyl sulfoxide (DMSO) solution: A fundamental study for development of the lithium–oxygen Battery. *J. Phys. Chem. C* **2015**, *119*, 12236–12250.
- (17) Choi, Y. M.; Abernathy, H.; Chen, H.-T.; Lin, M. C.; Liu, M. Characterization of O<sub>2</sub>–CeO<sub>2</sub> interactions using in situ Raman spectroscopy and First-principle calculations. *Chem. Phys. Chem.* **2006**, *7*, 1957–1963.
- (18) Frith, J. T.; Russell, A. E.; Garcia-Araez, N.; Owen, J. R. An in-situ Raman study of the oxygen reduction reaction in ionic liquids. *Electrochim. Commun.* **2014**, *46*, 33–35.
- (19) Zhu, J.; Yang, J.; Zhou, J.; Zhang, T.; Li, L.; Wang, J.; Nuli, Y. A stable organic–inorganic hybrid layer protected lithium metal anode for long-cycle lithium–oxygen batteries. *J. Power Sources* **2017**, *366*, 265–269.
- (20) Chen, X. J.; Bevara, V. V.; Andrei, P.; Hendrickson, M.; Plichta, E. J.; Zheng, J. P. Combined effects of oxygen diffusion and electronic resistance in Li–Air batteries with carbon nanofiber cathodes. *J. Electrochem. Soc.* **2014**, *161*, A1877–A1883.
- (21) Li, Z.; Du, F.; Bie, X.; Zhang, D.; Cai, Y.; Cui, X.; Wang, C.; Chen, G.; Wei, Y. Electrochemical kinetics of the Li-[Li<sub>0.23</sub>Co<sub>0.3</sub>Mn<sub>0.47</sub>]O<sub>2</sub> cathode material studied by GITT and EIS. *J. Phys. Chem. C* **2010**, *114*, 22751–22757.
- (22) Bardenhagen, I.; Yezerska, O.; Augustin, M.; Fenske, D.; Wittstock, A.; Bäumer, M. In situ investigation of pore clogging during discharge of a Li/O<sub>2</sub> battery by electrochemical impedance spectroscopy. *J. Power Sources* **2015**, *278*, 255–264.
- (23) Xiao, J.; Wanga, D.; Xu, W.; Wang, D.; Williford, R. E.; Liu, J.; Zhang, J.-G. Optimization of air electrode for Li/Air batteries. *J. Electrochem. Soc.* **2010**, *157*, A487–A492.
- (24) Li, Q.; Cao, R.; Cho, J.; Wu, G. Nanostructured carbon-based cathode catalysts for nonaqueous lithium–oxygen batteries. *Phys. Chem. Chem. Phys.* **2014**, *16*, 13568–13582.
- (25) Veith, G. M.; Nanda, J.; Delmau, L. H.; Dudney, N. J. Influence of lithium salts on the discharge chemistry of Li–Air Cells. *J. Phys. Chem. Lett.* **2012**, *3*, 1242–1247.
- (26) Lu, Y.-C.; Gasteiger, H. A.; Shao-Horn, Y. Catalytic activity trends of oxygen reduction reaction for nonaqueous Li–Air Batteries. *J. Am. Chem. Soc.* **2011**, *133*, 19048–19051.
- (27) Marinaro, M.; Theil, S.; Jörissen, L.; Wohlfahrt-Mehrens, M. New insights about the stability of lithium bis(trifluoromethane)sulfonimide-tetraglyme as electrolyte for Li–O<sub>2</sub> batteries. *Electrochim. Acta* **2013**, *108*, 795–800.
- (28) Messaggi, F.; Ruggeri, I.; Genovese, D.; Zaccheroni, N.; Arbizzani, C.; Soavi, F. Oxygen redox reaction in lithium-based electrolytes: from salt-in-solvent to solvent-in-salt. *Electrochim. Acta* **2017**, *245*, 296–302.
- (29) Markus, I. M.; Jones, G.; García, J. M. Investigation of electrolyte concentration effects on the performance of lithium–oxygen batteries. *J. Phys. Chem. C* **2016**, *120*, 5949–5957.
- (30) Li, F.; Zhang, T.; Yamada, Y.; Yamada, A.; Zhou, H. Enhanced cycling performance of Li–O<sub>2</sub> batteries by the optimized electrolyte concentration of LiTFSA in glymes. *Adv. Energy Mater.* **2013**, *3*, 532–538.
- (31) Gittleson, F. S.; Jones, R. E.; Ward, D. K.; Foster, M. E. Oxygen solubility and transport in Li–air battery electrolytes: establishing criteria and strategies for electrolyte design. *Energy Environ. Sci.* **2017**, *10*, 1167–1179.
- (32) Klassen, B.; Aroca, R.; Nazri, M.; Nazri, G. A. Raman spectra and transport properties of lithium perchlorate in ethylene carbonate based binary solvent systems for lithium batteries. *J. Phys. Chem. B* **1998**, *102*, 4795–4801.
- (33) Xu, W.; Xiao, J.; Zhang, J.; Wang, D.; Zhang, J.-G. Optimization of nonaqueous electrolytes for primary lithium/air batteries operated in ambient environment. *J. Electrochem. Soc.* **2009**, *156*, A773–A779.
- (34) Liu, B.; Xu, W.; Yan, P.; Sun, X.; Bowden, M. E.; Read, J.; Qian, J.; Mei, D.; Wang, C. M.; Zhang, J. G. Enhanced cycling stability of rechargeable Li–O<sub>2</sub> batteries using high-concentration electrolytes. *Adv. Funct. Mater.* **2016**, *26*, 605–613.
- (35) Liu, Y.; Suo, L.; Lin, H.; Yang, W.; Fang, Y.; Liu, X.; Wang, D.; Hu, Y.-S.; Han, W.; Chen, L. Novel approach for a high-energy-density Li–air battery: tri-dimensional growth of Li<sub>2</sub>O<sub>2</sub> crystals tailored by electrolyte Li<sup>+</sup> ion concentrations. *J. Mater. Chem. A* **2014**, *2*, 9020–9024.
- (36) Padbury, R.; Zhang, X. Lithium–oxygen batteries—limiting factors that affect performance. *J. Power Sources* **2011**, *196*, 4436–4444.
- (37) Kim, B. G.; Kim, H.-J.; Back, S.; Nam, K. W.; Jung, Y.; Han, Y.-K.; Choi, J. W. Improved reversibility in lithium–oxygen battery: understanding elementary reactions and surface charge engineering of metal alloy catalyst. *Sci. Rep.* **2014**, *4*, No. 4225.
- (38) Yao, X.; Dong, Q.; Cheng, Q.; Wang, D. Why do lithium–oxygen batteries fail: parasitic chemical reactions and their synergistic effect. *Angew. Chem., Int. Ed.* **2016**, *55*, 11344–11353.
- (39) Elia, G. A.; Hassoun, J.; Kwak, W.-J.; Sun, Y.-K.; Scrosati, B.; Mueller, F.; Bresser, D.; Passerini, S.; Oberhuber, P.; Tsiorvas, N.; Reiter, J. An advanced lithium–air battery exploiting an ionic liquid-based electrolyte. *Nano Lett.* **2014**, *14*, 6572–6577.
- (40) Burke, C. M.; Pande, V.; Khetan, A.; Viswanathan, V.; McCloskey, B. D. Enhancing electrochemical intermediate solvation through electrolyte anion selection to increase nonaqueous Li–O<sub>2</sub> battery capacity. *Proc. Natl. Acad. Sci. U.S.A.* **2015**, *112*, 9293–9298.